HERMETIC PACKAGES AND FEEDTHROUGHS FOR NEURAL PROSTHESES

Quarterly Progress Report # 7

(Contract NIH-NINCDS-N01-NS-4-2319)

(Contractor: The Regents of the University of Michigan)

For the Period:

April-June 1996

Submitted to the

Neural Prosthesis Program
National Institute of Neurological Disorders and Stroke
National Institutes of Health

By the

Center For Integrated Sensors and Circuits
Department of Electrical Engineering and Computer Science
University of Michigan
Ann Arbor, Michigan 48109-2122

Program Personnel:

UNIVERSITY OF MICHIGAN
Professor Khalil Najafi: Principal Investigator

Graduate Student Research Assistants:
Mr. Anthony Coghlan: RF Telemetry & Microstimulator Assembly
Mr. Mehmet Dokmeci: Packaging and Accelerated Testing
Mr. Jeffrey Von Arx: Electrode and Package Fabrication/Testing

VANDERBILT UNIVERSITY
Professor David L. Zealear, Principal Investigator

July 1996

SUMMARY

During the past quarter we continued testing of glass packages under accelerated conditions, redesigned the circuitry for the single-channel microstimulator and obtained masks for its fabrication, and completed the fabrication of a new run of silicon substrates for use in future package testing.

Our most significant package testing results to date are those obtained from a series of silicon-glass packages that have been soaking in DI water at 85°C and 95°C for more than a year. We reported in the last progress report that the last package that was soaking at 95°C had failed. There were also 4 packages that were soaking at 85°C. All these four packages are still dry and under test. Of the original 10 packages, the longest going sample has reached a maximum of 671 days at 85°C and 484 days at 95°C. We have calculated a worst case mean time to failure of 340 days for the samples at 85°C (assuming that all failed today), and of 119 days for the samples soaking at 95°C. The worst case MTTF at body temperature based on these tests is 386 years. The activation energy is calculated to be about 1.2eV. These tests have been very encouraging and clearly indicate the packages can last for many years in aqueous environments.

In addition to these tests in DI water, we also continued soaking the new ultrasonically-machined glass capsules in ***saline*** at the above two temperatures. These new glass capsules were bonded to thick silicon substrates. We had started soaking a total of 28 packages in the previous quarter, namely 17 at 85°C and 11 at 95°C. Out of these 11 packages that were tested at 95°C all had failed before. From the 17 packages that were started at 85°C, we had 2 dry packages at the beginning of this quarter. Both of these packages have recently failed. Packages that were soaked at 95°C all failed at various points in time, exclusively due to corrosion and dissolution of the polysilicon bonding layer in saline. Nonetheless, we have calculated an average lifetime of about 38 days for these preliminary soaks at 95°C, and 115.6 days at 85°C. Using these values, one can calculate a MTTF of about 177 years at 37°C. As mentioned above, the primary problem with these soak tests in saline at 95°C is dissolution of the deposited thin films. This was verified this last quarter by soaking three packages in saline at 95°C, while coating the polysilicon surface with silicone rubber. One of these packages failed after 156 days, and the two remaining samples are still dry after 225 days. We have also analyzed all failed packages visually and have clearly noticed a leakage path due to polysilicon dissolution in all of these samples. We will continue to conduct additional tests using a new set of silicon substrates that have just been fabricated.

We also have had 4 packages soaking at room temperature in saline. The longest lasting package has been soaking for 572 days, and we have obtained an average soak period of 483 days for all packages at room temperature. We will continue to observe these packages for any sign of leakage.

Finally, during the past quarter we finished the design and optimization of a new receiver circuit. As mentioned before, due to the large power dissipation in the single-channel circuitry, we could not operate the microstimulator within the entire volume of the transmitter coil reliably. A new circuitry has been designed, simulated, and layed out and fabrication of the new devices will begin shortly. The new design consumes 45% less power, is much more tolerant to variations in process parameters, and provides a much more stable output current compared to the current circuitry. Simulations of the telemetry link indicate that the microstimulator should be able to operate within the 9cm diameter transmitter coil and deliver the required current levels. This circuitry together with a slightly modified version of the multichannel microstimulator will be fabricated in the coming quarter.

1. INTRODUCTION

This project deals with the development of hermetic, biocompatible micropackages and feedthroughs for use in a variety of implantable neural prostheses for sensory and motor handicapped individuals. The project also aims at continuing work on the development of a telemetrically powered and controlled neuromuscular microstimulator for functional electrical stimulation. The primary objectives of the project are: 1) the development and characterization of hermetic packages for miniature, silicon-based, implantable three-dimensional structures designed to interface with the nervous system for periods of up to 40 years; 2) the development of techniques for providing multiple sealed feedthroughs for the hermetic package; 3) the development of custom-designed packages and systems used in chronic stimulation or recording in the central or peripheral nervous systems in collaboration and cooperation with groups actively involved in developing such systems; and 4) establishing the functionality and biocompatibility of these custom-designed packages in *in-vivo* applications. Although the project is focused on the development of the packages and feedthroughs, it also aims at the development of inductively powered systems that can be used in many implantable recording/stimulation devices in general, and of multichannel microstimulators for functional neuromuscular stimulation in particular.

Our group here at the Center for Integrated Sensors and Circuits at the University of Michigan has been involved in the development of silicon-based multichannel recording and stimulating microprobes for use in the central and peripheral nervous systems. More specifically, during the past two contract periods dealing with the development of a single-channel inductively powered microstimulator, our research and development program has made considerable progress in a number of areas related to the above goals. A hermetic packaging technique based on electrostatic bonding of a custom-made glass capsule and a supporting silicon substrate has been developed and has been shown to be hermetic for a period of at least a few years in salt water environments. This technique allows the transfer of multiple interconnect leads between electronic circuitry and hybrid components located in the sealed interior of the capsule and electrodes located outside of the capsule. The glass capsule can be fabricated using a variety of materials and can be made to have arbitrary dimensions as small as 1.8mm in diameter. A multiple sealed feedthrough technology has been developed that allows the transfer of electrical signals through polysilicon conductor lines located on a silicon support substrate. Many feedthroughs can be fabricated in a small area. The packaging and feedthrough techniques utilize biocompatible materials and can be integrated with a variety of micromachined silicon structures.

The general requirements of the hermetic packages and feedthroughs to be developed under this project are summarized in Table 1. Under this project we will concentrate our efforts to satisfy these requirements and to achieve the goals outlined above. There are a variety of neural prostheses used in different applications, each having different requirements for the package, the feedthroughs, and the particular system application. The overall goal of the program is to develop a miniature hermetic package that can seal a variety of electronic components such as capacitors and coils, and integrated circuits and sensors (in particular electrodes) used in neural prostheses. Although the applications are different, it is possible to identify a number of common requirements in all of these applications in addition to those requirements listed in Table 1. The packaging and feedthrough technology should be capable of:

1- protecting non-planar electronic components such as capacitors and coils, which typically have large dimensions of about a few millimeters, without damaging them;
2- protecting circuit chips that are either integrated monolithically or attached in a hybrid fashion with the substrate that supports the sensors used in the implant;
3- interfacing with structures that contain either thin-film silicon microelectrodes or conventional microelectrodes that are attached to the structure;

Table 1: General Requirements for Miniature Hermetic Packages and Feedthroughs for Neural Prostheses Applications

Package Lifetime:
≥ 40 Years in Biological Environments @ 37°C

Packaging Temperature:
≤360°C

Package Volume:
10-100 cubic millimeters

Package Material:
Biocompatible
Transparent to Light
Transparent to RF Signals

Package Technology:
Batch Manufactureable

Package Testability:
Capable of Remote Monitoring
In-Situ Sensors (Humidity & Others)

Feedthroughs:
At Least 12 with ≤125μm Pitch
Compatible with Integrated or Hybrid Microelectrodes
Sealed Against Leakage

Testing Protocols:
In-Vitro Under Accelerated Conditions
In-Vivo in Chronic Recording/Stimulation Applications

We have identified two general categories of packages that need to be developed for implantable neural prostheses. The first deals with those systems that contain large components like capacitors, coils, and perhaps hybrid integrated circuit chips. The second deals with those systems that contain only integrated circuit chips that are either integrated in the substrate or are attached in a hybrid fashion to the system.

Figure 1 shows our general proposed approach for the package required in the first category. This figure shows top and cross-sectional views of our proposed approach here. The package is a glass capsule that is electrostatically sealed to a support silicon substrate. Inside the glass capsule are housed all of the necessary components for the system. The electronic circuitry needed for any analog or digital circuit functions is either fabricated on a separate circuit chip that is hybrid mounted on the silicon substrate and electrically connected to the silicon substrate, or integrated monolithically in the support silicon substrate itself. The attachment of the hybrid IC chip to the silicon substrate can be performed using a number of different technologies such as simple wire bonding between pads located on each substrate, or using more sophisticated techniques such as flip-chip solder reflow or tab bonding. The larger capacitor or microcoil components are mounted on either the substrate or the IC chip using appropriate epoxies or solders. This completes the assembly of the electronic components of the system and it should be possible to test the system electronically at this point before the package is completed. After testing, the system is packaged by placing the glass capsule over the entire system and bonding it to the silicon substrate using an electrostatic sealing process. The cavity inside the glass package is now hermetically sealed against the outside environment. Feedthroughs to the outside world are provided using the grid-feedthrough technique discussed in previous reports. These feedthroughs transfer the electrical signals between the electronics inside the package and various elements outside of the package. If the package has to interface with conventional microelectrodes, these microelectrodes can be attached to bonding pads located outside of the package; the bond junctions will have to be protected from the external environment using various polymeric encapsulants. If the package has to interface with on-chip electrodes, it can do so by integrating the electrode on the silicon support substrate. Interconnection is simply achieved using on-chip polysilicon conductors that make the feedthroughs themselves. If the package has to interface with remotely located recording or stimulating electrodes that are attached to the package using a silicon ribbon cable, it can do so by integrating the cable and the electrodes again with the silicon support substrate that houses the package and the electronic components within it.

Figure 2 shows our proposed approach to package development for the second category of applications. In these applications, there are no large components such as capacitors and coils. The only component that needs to be hermetically protected is the electronic circuitry. This circuitry is either monolithically fabricated in the silicon substrate that supports the electrodes (similar to the active multichannel probes being developed by the Michigan group), or is hybrid attached to the silicon substrate that supports the electrodes (like the passive probes being developed by the Michigan group). In both of these cases the package is again another glass capsule that is electrostatically sealed to the silicon substrate. Notice that in this case, the glass package need not be a high profile capsule, but rather it need only have a cavity that is deep enough to allow for the silicon chip to reside within it. Note that although the silicon IC chip is originally 500μm thick, it can be thinned down to about 100μm, or can be recessed in a cavity created in the silicon substrate itself. In either case, the recess in the glass is less than 100μm deep (as opposed to several millimeters for the glass capsule). Such a glass package can be easily fabricated in a batch process from a larger glass wafer.

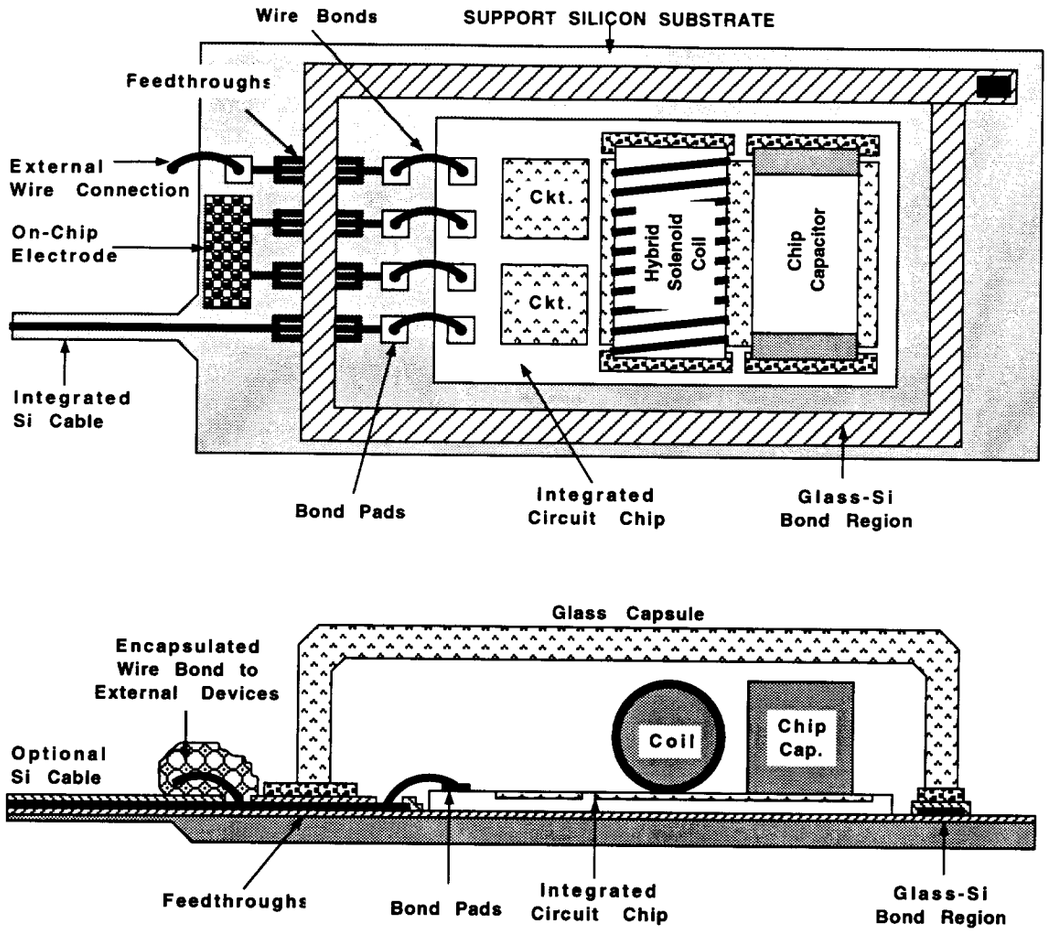

Figure 1: A generic approach for packaging implantable neural prostheses that contain a variety of components such as chip capacitors, microcoils, and integrated circuit chips. This packaging approach allows for connecting to a variety of electrodes.

We believe the above two approaches address the needs for most implantable neural prostheses. Note that both of these techniques utilize a silicon substrate as the supporting base, and are not directly applicable to structures that use other materials such as ceramics or metals. Although this may seem a limitation at first, we believe that the use of silicon is, in fact, an advantage because it provides several benefits. First, it is biocompatible and has been used extensively in biological applications. Second, there is a great deal of effort in the IC industry in the development of multi-chip modules (MCMs), and many of these efforts use silicon supports because of the ability to form high density interconnections on silicon using standard IC fabrication techniques. Third, many present and future implantable probes are based on silicon micromachining technology; the use of our proposed packaging technology is inherently compatible with most of these probes, which simplifies the overall structure and reduces its size.

Once the above packages are developed, we will test them in biological environments by designing packages for specific applications. One of these applications is in recording neural activity from cortex using silicon microprobes developed by the Michigan group under separate contracts. The other involves the chronic stimulation of muscular tissue using a multichannel microstimulator for the stimulation of the paralyzed larynx. This application has been developed at Vanderbilt University. Once the device is built, it will be used by our colleagues at Vanderbilt to perform both biocompatibility tests and functional tests to determine package integrity and suitability and device functionality for the reanimation of the paralyzed larynx. The details of this application will be discussed in future progress reports.

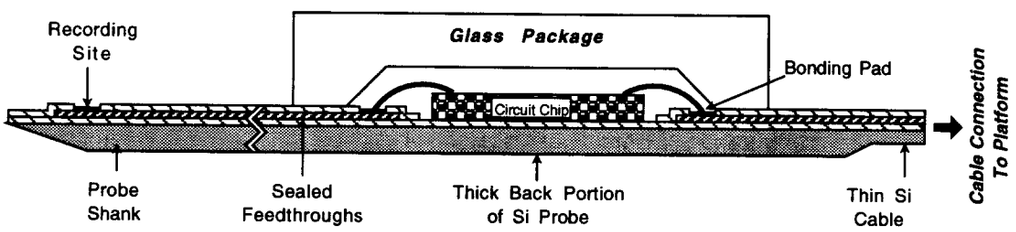

Figure 2: Proposed packaging approach for implantable neural prostheses that contain electronic circuitry, either monolithically fabricated in the probe substrate or hybrid attached to the silicon substrate containing microelectrodes.

2. ACTIVITIES DURING THE PAST QUARTER

2.1 Hermetic Packaging

Over the past few years we have developed a biocompatible hermetic package with high density, multiple feedthroughs. This technology utilizes electrostatic bonding of a custom-made glass capsule to a silicon substrate to form a hermetically sealed cavity, as shown in Figure 3. Feedthrough lines are obtained by forming closely-spaced polysilicon lines and planarizing them with LTO and PSG. The PSG is reflowed at 1100°C for 2 hours in steam to form a planarized surface. A passivation layer of oxide/nitride/oxide is then deposited on top to prevent direct exposure of PSG to moisture. A layer of fine-grain polysilicon (surface roughness 50Å rms) is deposited and doped to act as the bonding surface. Finally, a glass capsule is bonded to this top polysilicon layer by applying a voltage of 2000V between the two for 10 minutes at 320 to 340°C, a temperature compatible with most hybrid components. The glass capsule can be either custom molded from Corning code #7740 glass, or can be batch fabricated using ultrasonic micromachining of #7740 glass wafers.

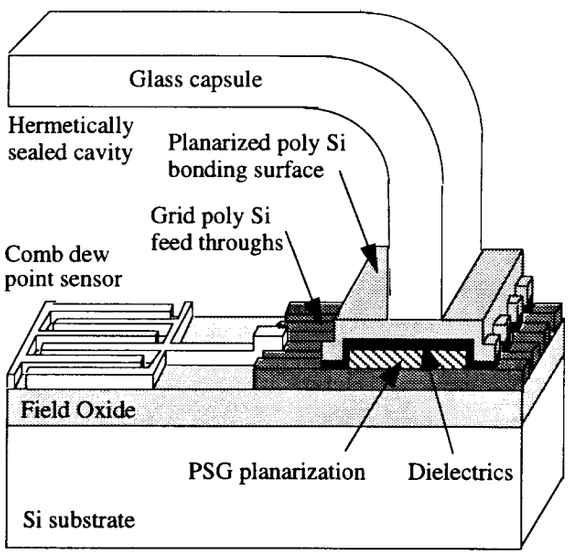

Figure 3: The structure of the hermetic package with grid feedthroughs.

During the past year we have electrostatically bonded and soak tested over one hundred and sixty of these packages. The packages successfully prevent leakage in soak tests at 95°C for over 4 months on average and at 85°C for almost 11 months on average both in deionized water. The bonding yield has varied between 85% to 72% (yield is defined as the percentage of packages which last more than 24 hours soaking in DI water), and preliminary in-vivo tests indicate that the package is biocompatible and rugged. Since a number of different types of packages have been tested, it is important to distinguish between these different packages that were being tested. Earlier tests, specifically the room temperature tests in phosphate buffered saline and the 85°C and the 95°C tests in deionized water, were performed with thinned silicon substrates (thinned down to about 150μm) using the custom molded glass capsules made from Corning code #7740 Pyrex glass. The more recent tests, namely the 85°C and 95°C tests in phosphate buffered saline, have been performed using silicon substrates having full thickness (about 500μm) and the ultrasonically micromachined glass capsules made of #7740 Pyrex glass wafers.

The following summarizes the results obtained to date and plans for the coming quarters in hermetic packaging.

2.1.1 Accelerated Soak Tests With The Ultrasonically-Machined Glass Capsules

In the past progress report we mentioned that 28 new packages have been made with the ultrasonically machined glass capsules bonded to full thickness silicon substrates. Seventeen of these packages have been soaked at 85° C and 11 of them have been soaked at 95°C, both in phosphate buffered saline. The samples at each temperature have been tested both electrically with the aid of dew point sensors inside the packages and also visually with the help of a microscope. These tests are performed every three to four days by taking the package out of its jar, cooling the sample down to room temperature and then making the measurement. The saline solution in each jar is changed daily in order to keep the concentration of the saline at a constant level. If the saline solution is not changed, at this high temperature the solution evaporates and changes the concentration of saline and hence not only leaves a residue on the glass capsules causing difficulty in visual inspection, but also enhances dissolution of the polysilicon bonding layer.

Tables 2 and 3 summarize the pertinent data from these tests. Due to the dissolution of the polysilicon bonding surface at this higher temperature, the soak tests at 95°C have come to a conclusion earlier than the 85°C tests. The longest lasting package in the 95°C tests has survived a total of 70 days. The average lifetime was calculated to be 38 days. Of the original 17 packages in the 85°C soak tests we had 2 packages that were dry at the beginning of this quarter. These 2 samples have recently failed after being soaked for 208 and 321 days in saline. From this data we have calculated a mean time to failure of 115.6 days for the samples soaking at 85°C. The calculations for the mean time to failures do not include the samples that have failed within 24 hours from the start of the tests because these failures are related to poor bonding between the polysilicon layer and the glass capsule which is caused by particulates and defects that reside on the bonding surface created during processing and also from alignment errors. The longest lasting sample in these 85°C tests has survived a total of 321 days. In the failure analysis section we will provide additional detail and information on this sample. Figures 4 and 5 show a summary plot of all of the long-term soak tests performed at 85°C and 95°C as a function of time, respectively.

As mentioned in past progress reports, most of our samples have failed due to the dissolution of the polysilicon layer. In order to reduce the dissolution of this polysilicon layer, we have prepared 3 packages and have coated the interface between the glass and the polysilicon layer with silicone rubber and then soaked them at 95°C (the temperature at which the dissolution of the polysilicon was the most severe). Since the packages have been treated differently we did not include these results in the above mentioned 11 samples. With the application of this coating the lifetime of the samples have improved significantly. The first sample has failed after surviving for 156 days in saline at 95° C. The remaining two are still dry after 225 days and are still being tested. For comparison, the longest lasting sample at 95°C had survived a total of 70 days from a sample set of 11 packages. Based on this test, and based on visual observations, it is clear that the dissolution of silicon at the higher temperature of 95°C is the main cause of failure and therefore limits the maximum temperature to which the samples can be accelerated. We should also add that while applying the polymer air bubbles get trapped between the polysilicon and glass interface and when the samples are soaked at a high temperature, the air expands and forms larger bubbles. As the sample is cooled down to room temperature during measurements, these bubbles disappear and this cycling process introduces a stress to the coating. With time, this heat cycling damages the coating and finally allows saline to penetrate to the polysilicon glass interface which starts the dissolution process. The failed

sample has analyzed and as expected shows a leakage path that extends across the bonding surface which strongly suggests that the sample has failed due to the dissolution of the polysilicon layer. We feel that by perfecting our technique in applying the silicone rubber to the interface and also by investigating other coatings we can reduce this dissolution process.

Table 2: Key data for 85°C soak tests in saline.

Number of packages in this study	17
Soaking solution	Saline
Failed within 24 hours (not included in MTTF)	3
Packages lost due to mishandling	0
Longest lasting packages so far in this study	321 days
Packages still under tests with no measurable room temperature condensation inside	0
Average lifetime to date (MTTF)	*115.6 days*

Table 3: Key data for 95°C soak tests in saline.

Number of packages in this study	11
Soaking solution	Saline
Failed within 24 hours (not included in MTTF)	5
Packages lost due to mishandling	0
Longest lasting packages so far in this study	70 days
Packages still under tests with no measurable room temperature condensation inside	0
Average lifetime to date (MTTF)	*38 days*

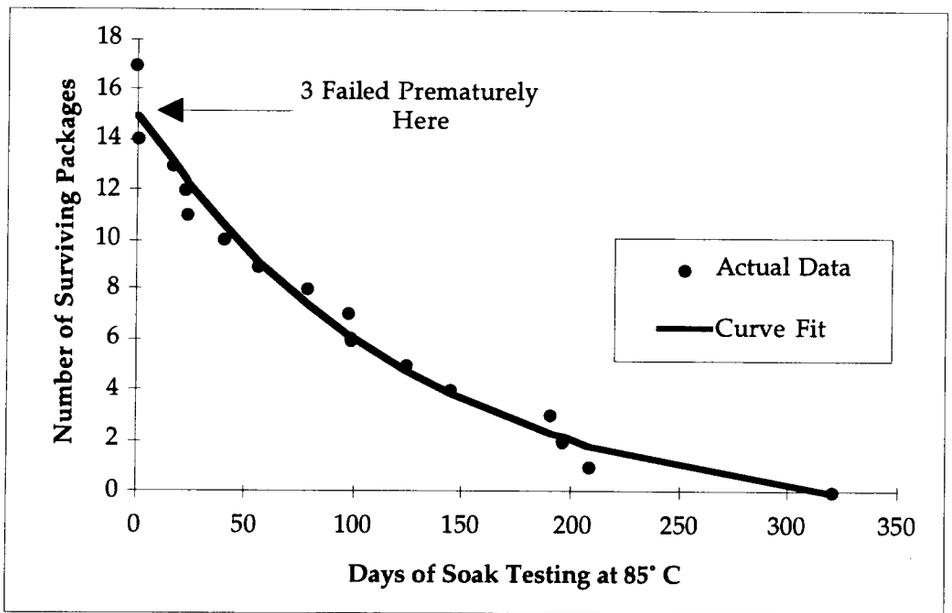

Figure 4: Summary of the lifetimes of the 17 packages which have been soak tested at 85° C in saline solution.

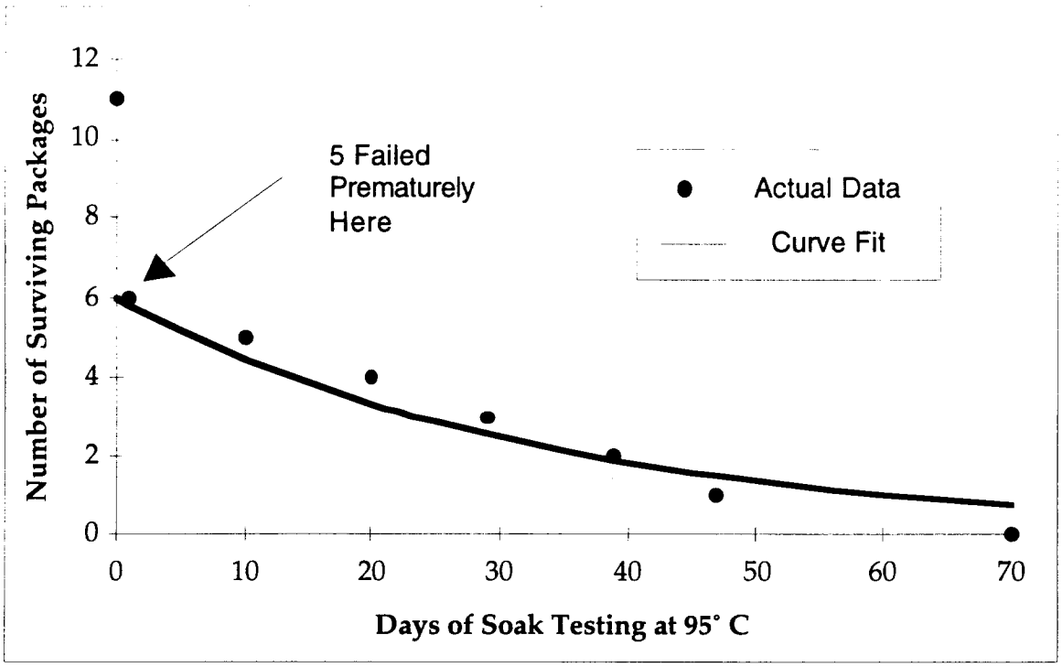

Figure 5: Summary of the lifetimes of the 11 packages which have been soak tested at 95°C in saline solution.

2.1.2 Interpretation of Long Term Soak Testing Results in Saline

Generally during accelerated testing, the mean time to failure (MTTF) is modeled by an Arrhenius processes (in the VLSI industry this model is used for failure due to diffusion, corrosion, mechanical stress, electromigration, contact failure, dielectric breakdown, and mobile ion/surface inversion). The generalized equation used in all these cases is given below where MTTF is the mean time to failure, A is a constant, ξ is the stress factor other than temperature, (such as pressure or relative humidity), n is the stress dependence, Q is the activation energy, K_B is Boltzman's constant, and T is the temperature in Kelvin.

$$MTTF = A \cdot \xi^{-n} \cdot e^{\left(\frac{Q}{K_B T}\right)}$$

For the accelerated soak tests that we have performed on the packages, there was no stressing factor other than temperature, so the x term drops out of the above equation. The resulting equation can be rewritten as a ratio of MTTFs as it is below. This is the model we are using to interpret the accelerated soak tests.

$$AF = \frac{MTTF_{Normal}}{MTTF_{Accelerated}} = e^{\frac{Q}{K_B}\left(\frac{1}{T_{Normal}} - \frac{1}{T_{Accelerated}}\right)}$$

By using the current MTTFs at 85°C and 95°C, we then calculate the activation energy (Q) and from this activation energy we proceed to obtain an acceleration factor (AF) for these tests, and then calculated the MTTF at body temperature. With the tests at 85°C having been completed this quarter, we can actually get a very close estimate of our lifetimes at 37° C. Performing this calculation yields:

$$MTTF\big|_{85°C} = 115.6\,Days \quad MTTF\big|_{95°C} = 38\,Days$$

Q=1.26eV, AF(95°C)=1693, AF(85°C)=558

$$MTTF\big|_{37°C} = 177\ Years$$

The activation energy of 1.26 eV is about what we expect for these packages. For comparison, corrosion is known to be one of the major failure mechanisms for plastic-encapsulated silicon chips, and the activation energy for corrosion of these standard plastic packages is well characterized and known to be about 0.7 to 0.9 eV. Hence our calculated average lifetime of 177 years at the body temperature is a fairly feasible lifetime. Note that this activation energy is also larger than that we presented in previous reports and is consistent with the values we calculated in DI water.

2.1.3 Ongoing Accelerated Soak Tests in Deionized Water

We have continued accelerated soak testing of the packages in DI water this quarter, and 20% of the packages in these tests have now surpassed one and a half year of accelerated testing still showing no sign of moisture penetration. Similar to the tests in saline, for these tests we have chosen temperature as the acceleration factor because it is an easy variable to control, and because moisture diffusion is a strong (exponential) function of temperature. We have been soaking 10 samples each at 95°C and 85°C in this series of tests. Table 4 and 5 summarize some pertinent data for these soak tests. Figure 6 summarizes the results so far from the 95°C soak tests and Figure 7 summarizes the results so far from the 85°C tests. These figures also list the causes of failure for individual packages when it is known, and they show a curve fit to our lifetime data to illustrate the general trend. The curve fit, however, only approximates the actual package lifetimes since some of our packages failed due to breaking during testing rather than due to leakage.

Of the original 10 packages in the 85°C soak tests there are still 4 with no sign of room temperature condensation with the longest one lasting for more than 671 days. The worst case mean time to failure for these tests have been calculated at 528 days excluding the handling errors. Since four of these packages have not failed we can only assume that all of them fail today and hence obtain a worst case mean time to failure value. The failure for these tests is

defined as the condensation at room temperature. The packages in these accelerated tests are monitored every few days for room temperature condensation both electrically by means of an integrated dew point sensor, and by visual inspection with the help of a microscope. Of the original 10 packages in the 95°C tests, the longest lasting package survived for a total of 484 days. The calculated mean time to failure of the packages are 135.7 days.

2.1.4 Interpretation of the Long Term Soak Testing Results in Deionized Water

The results obtained for the packages soaking in DI water can be analyzed similar to tests in saline, just discussed above. Here, the same model is used and temperature is used as the accelerating factor.

By using the current MTTFs at 85°C and 95°C, we can easily calculate the activation energy (Q) and from this activation energy we can proceed to obtain an acceleration factor (AF) for these tests, and then calculate the MTTF at body temperature. Since the tests at 85°C are still in progress we cannot accurately determine the activation energy in our tests. Also until all of the samples show leakage, we cannot obtain the MTTF at the accelerated temperatures. We can, however, obtain worst case MTTFs for the 85°C soak tests by assuming that all the remaining packages in this test show leakage today. This worst case MTTF can be used to calculate the worst case activation energy, and hence the worst case MTTF at body temperature. Performing this calculation yields:

Table 4: Key data for 95°C soak tests in DI water.

Number of packages in this study	10
Soaking solution	DI water
Failed within 24 hours (not included in MTTF)	1
Packages lost due to mishandling	2
Longest lasting packages in this study	484 days
Packages still under tests with no measurable room temperature condensation inside	0
Average lifetime to date (MTTF) including losses attributed to mishandling	*118.7 days*
Average lifetime to date (MTTF) not including losses attributed to mishandling	*135.7 days*

Table 5: Key data for 85°C soak tests in DI water.

Number of packages in this study	10
Soaking solution	DI water
Failed within 24 hours (not included in MTTF)	2
Packages lost due to mishandling	3
Longest lasting packages so far in this study	671 days
Packages still under tests with no measurable room temperature condensation inside	4
Average lifetime to date (MTTF) including losses attributed to mishandling	*340 days*
Average lifetime to date (MTTF) not including losses attributed to mishandling	*528 days*

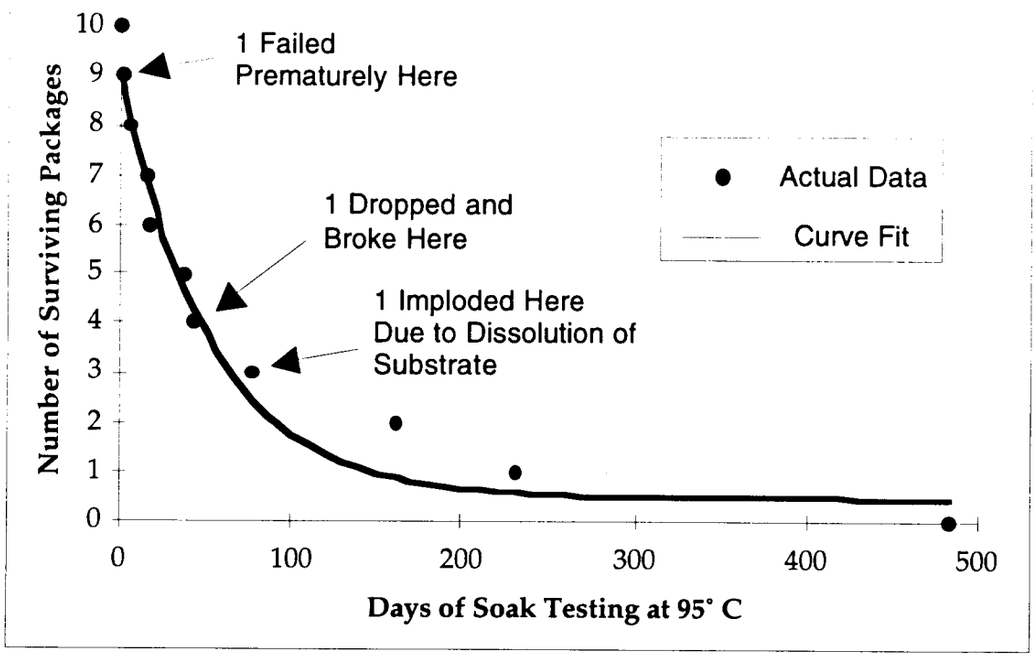

Figure 6: Summary of the lifetimes of the 10 packages which have been soak tested at 95° C in DI water.

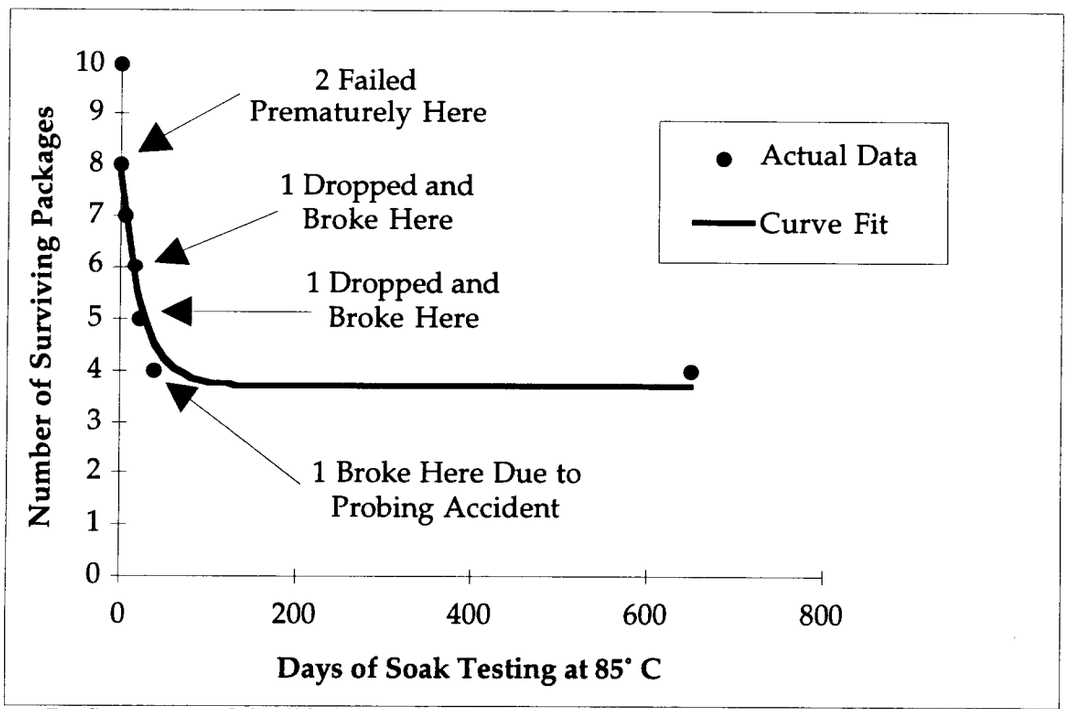

Figure 7: Summary of the lifetimes of the 10 packages which have been soak tested at 85° C in DI water.

$$MTTF|_{85°C} = 340\,Days \quad MTTF|_{95°C} = 118.7\,Days$$

Q=1.2eV, AF(95°C)=1188, AF(85°C)=413

$$MTTF|_{37°C} = 386\ Years$$

We call this average lifetime at body temperature of 386 years the worst case lifetime because every extra day that the remaining 85°C packages last increases this projected lifetime. Moreover, the activation energy calculated from the saline tests mentioned in the previous section was 1.26eV which is very close to the one found in these deionized water tests. It should also be noted that we have included every single sample in the 85°C and 95°C soak tests in this calculation except the 15% which failed in the first day (we assume that these early failures can be screened for). However some of these capsules failed due to mishandling during testing, rather than due to actual leakage of the package. If we disregard the samples that we have attributed failure due to mishandling, we obtain a somewhat longer mean time to failure:

$$MTTF|_{85°C} = 528\,Days \quad MTTF|_{95°C} = 135.7\,Days$$

Q=1.54eV, AF(95°C)=8833, AF(85°C)=2275

$$MTTF|_{37°C} = 3290\ Years$$

The above activation energy of 1.54eV is higher than what we expect for these packages mainly because of the fact that the standard plastic packages it is typical to have activation energies of about 0.7 to 0.9 eV. However, these results so far clearly indicate that results from the saline soak tests and the DI water tests are producing approximately the same activation energies, which is encouraging. We will continue to perform additional tests and collect more data to further verify these results.

2.1.5 Ongoing Room Temperature Soak Tests

We have continued the soak tests with the glass capsules bonded to thinned silicon substrates at room temperature in phosphate buffered saline solution. Table 6 below summarizes the pertinent data from these soak tests. We have started these soak tests as a control set to accompany our accelerated tests. We hope to include few samples from each fabrication run into this set and increase the number of samples soaking at this temperature. We have consistently observed in these tests that at room temperature we are below the activation energy required to cause dissolution and hence we have not yet observed any dissolution related failures. Out of the 6 samples that we have started, 1 failed within 24 hours due to alignment and process related defects, a second sample has failed after 160 days due to a handling error and the remaining 4 packages have shown no sign of moisture either measured electrically or observed visually after an average of 483 days of soaking and they are still under test. The longest going sample has reached a total of 572 days and is still dry.

Table 6: Data for room temperature soak tests in saline solution.

Number of packages in this study	6
Soaking solution	Saline
Failed within 24 hours (not included in MTTF)	1
Longest lasting packages so far in this study	572 days
Packages still under tests with no measurable room temperature condensation inside	4
Average lifetime to date (MTTF)	*483 days*

2.1.6 Fabrication of New Substrates

We have now completed the fabrication run of a new set of silicon substrates to be used with the ultrasonically machined glass capsules. We have inspected the bonding surface of these samples and the bonding surface seems fairly planar. The wafers are diced and we are in the process of preparing more packages for soak testing. We are also preparing more dummy packages with sensors for our collaborators at Vanderbilt University and also for other interested users. Another set of substrates are being reserved for the actual implants. With this current run, we hope to start a new set of soak tests at 3 different temperatures in saline solution as soon as possible. We will include the results of these tests in our next progress report.

2.1.7 Failure Analysis of the Samples That Have Failed During This Quarter

The two samples that have failed during this term have been thoroughly analyzed under a microscope and a SEM. One sample that has lasted for 208 days in saline solution at 85°C has been kept in the solution for a longer period of time to enhance the attack of saline and also to get better view of the dissolution by the saline solution. Figure 8 below shows a corner of the bonding surface with the left side severely attacked by the saline solution. The amount of polysilicon that is being dissolved (the darker regions) extends almost half way on the average across the bonding region. Close to the bottom right of the picture is the presence of a main leakage path for this sample. There is another relatively smaller leakage path which is next to this one, but it is formed some time after the main one as the sample was kept in the saline solution.

An interesting phenomenon is observed at the inner edge of the bonding region in which the polysilicon is also being attacked by saline from the inside of the package. We have expected and generally observed dissolution of the polysilicon layer starting from the outside and proceeding towards the inside of the package similar to the one seen in Figure 8. However, since this package was kept in the saline solution longer, the solution penetrated into the package and started to cause corrosion from the inside of the package. A similar picture is taken from another location of the same sample. Figure 9 shows a typical example of such a site in which the dissolution has commenced from the inside of the sample and has progressed towards the outside in an almost circular manner. The dissolution at the outer edges (to the left of the figure) is also apparent but much less than the inner one. We attribute this phenomenon to the fact that this sample had a gross leak and the amount of saline inside the package was significant enough that at the locations where the polysilicon to the glass bond was weak due to particulates, it attacked the polysilicon at a faster rate. This sample was later diced in several locations to zoom into the interface between the polysilicon and the glass capsule. The SEM micrograph in Figure 10 displays a general view of such an interface from the same sample.

Figure 8: The bonding region of a sample that has failed after being soaked for 208 days at 85° C in saline solution.

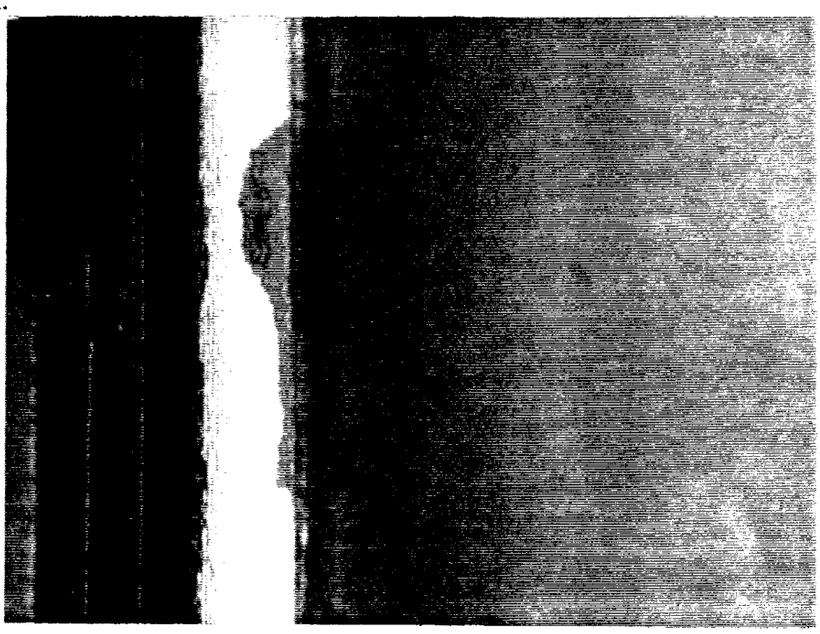

Figure 9: Another location of the bonding surface of the sample that has failed after being soaked for 208 days at 85°C in the saline solution.

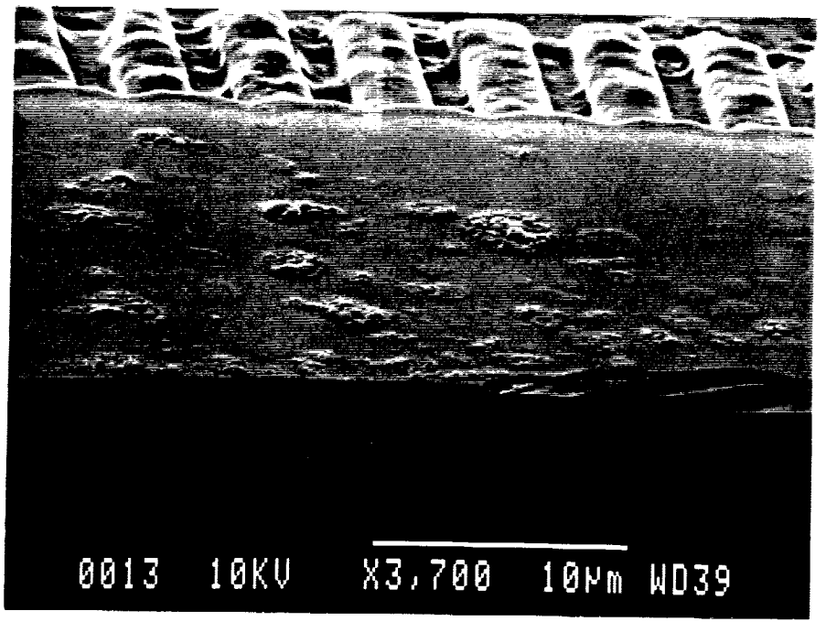

Figure 10: The SEM cross-section of the bonding region.

In this SEM micrograph we see that the polysilicon feedthroughs that originate from the top of the picture extend towards the front and one can notice their cross sections just below the top polysilicon bonding layer. We have also scanned the edge below the entire bonding region of this sample and did not observe any dissolution of the feedthrough lines. This justifies the theory that the polysilicon feedthroughs are well encapsulated and are not etched in the package that has been soaked for more than 208 days at 85° C in the saline solution. We have carefully inspected this sample, but found no evidence of any other failure mechanism than the one shown in Figure 8 for this sample. Moreover, we would like to distinguish these results from some of the observations made in the past progress report which was showing the dissolution of the feedthroughs. However, the difference was in that sample the substrate did not have a glass capsule, in other words the substrate was soaked with no covering glass package. Moreover, that sample was soaked in saline solution at 95°C for 139 days. Another sample that has lasted for 321 days has been inspected with the help of a microscope and Figure 11 below shows a corner of its bonding region. The remainder of the bonding region has been carefully inspected and no evidence of other leakage paths has been found. This leakage path and the inexistence of any other paths or dissolved layers suggests that the sole failure mode for our packages is the dissolution of top polysilicon layer in the saline solution. The amount of discoloration (dissolution of the top bonding polysilicon layer) has been carefully observed during our visual inspection performed every three to four days. This discoloration has progressed from a little circle to a major leakage path during the duration of our tests which is very similar to our observations in all of the other samples. In the coming quarter we will start new tests with our recent fabrication run and will report our findings from those tests.

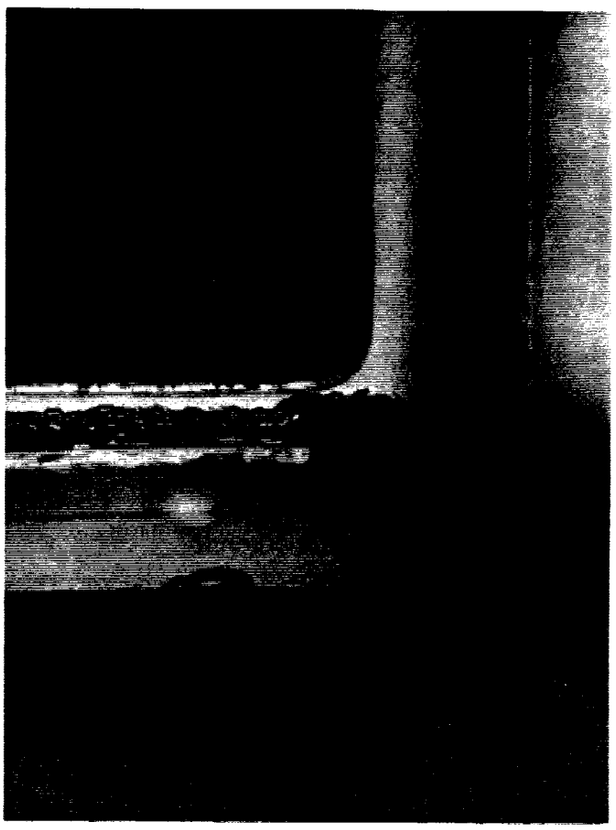

Figure 11: The leakage path of a sample that has leaked after 321 days in saline solution at 85°C.

2.2 Single-Channel Microstimulator Redesign

As mentioned in the previous quarterly report, we had been having difficulty in reliably powering the single-channel microstimulator. The difficulties were fundamentally in two areas: reception of adequate power from a reasonable, realistic telemetry link; and delivery of a stable, predictable stimulus current. Work this quarter has concentrated on the solution of these difficulties so that delivery of consistently reliable microstimulators may begin as soon as possible.

It was observed that in order to reliably operate the microstimulator, the device must receive at least 12.5V or so, preferably 15-20V, since there are both 8V and 4V supplies on chip and there will be some voltage drop through the rectifier bridge and voltage regulation circuitry. However, these voltage levels, even the lower ones, proved hard to receive unless the coupling of the telemetric link was increased by using either smaller transmitter coil diameters that were not practical for a wide range of applications (6cm diam. or less) or larger diameter receiver coils (1.5-2mm) that would not fit inside the current microstimulator package. In general a combination of these two improvements worked most reliably. Of course, microstimulators encapsulated in silicone rubber and utilizing larger diameter receiver coils would still be useful for short term applications or applications in which the size of the package is not as critical. Nonetheless, it was clear that for the larger scale assembly of reliably working microstimulators, an alternative solution should be found to this problem.

Furthermore, it was observed that the stimulus current generator of the single-channel microstimulator tended to vary undesirably from the expected 10mA. Theoretically, the system should have been able to deliver this 10mA stably through loads of up to roughly 800Ω as limited by the 8V compliance voltage. Under probe station and telemetric tests, it was observed that the stimulus current would increase dramatically across lower resistive loads (100-300Ω range), reaching as high as 15mA. These results were also seen under extensive simulation of this BiCMOS output stage using SPICE type simulators and device model files based on our fabrication process. These model files, unfortunately, did not exist when this stimulus generation block was first designed. The correspondence between modeled and observed behavior was a welcome observation, in any case.

The stimulus current generator of the multichannel microstimulator is an all CMOS stage that has been shown to deliver stable current pulses to a wide range of loads (limited, of course, by the compliance voltage). The design has several advantages over the single channel microstimulator's present BiCMOS stimulus generator. One of these is a higher compliance voltage, because the driver device is a MOS transistor operated in the linear region. In the BiCMOS stage, the BJT driver must be kept from going into saturation, or else the current delivered will diminish. Although the MOS driver is quite large for a typical MOS device, the complete MOS stimulus stage still occupies less overall area than its BiCMOS counterpart. Another tremendous advantage is adjustability of the stimulus current levels. In the multichannel device, the current amplitude is software programmable through the incoming data to deliver one of seven levels up to a maximum of 10mA. We decided to modify this output stage for use in the single channel microstimulator as well.

Thus several significant changes have been made, principally to the single channel microstimulator but also to some degree to the multichannel device. In the single channel device these changes have primarily been in the voltage regulation circuitry and in the stimulus generation circuitry. Their principal purpose has been to reduce the overall power consumption in the device and to produce a more stable and predictable output stimulus current. Small parallel changes have been made in the multichannel device. In addition, an improved envelope detector has been incorporated into one version of the single channel microstimulator and the multichannel microstimulator. A more detailed explanation of these changes will now follow.

Voltage Regulation / Power Supplies

Table 7 presents a detailed breakdown of the current consumption of the various generations of microstimulator. From this it can be seen that in the present single channel device, most of the current consumption is in the voltage regulators / power supplies. Even in the multichannel device, the current consumption in the regulators could be reduced somewhat. In the single channel device, the high current consumption resulted from the necessity to break down fairly large Zener diodes to produce a stable reference voltage. The breakdown current furthermore exhibited a nearly direct linear relationship with the received voltage level, at least in the 8V supply, because the Zener diodes were tied to the rectified input through a large (50kΩ) resistor. This resistor in itself consumed a large die area, also. The multichannel device produced the Zener breakdown current by using a stable current mirror instead of this direct supply dependence, thus reducing the current consumed considerably. It also used Zener diodes with roughly one-fifth the breakdown current, though these diodes were not properly characterized when the multichannel device was first designed, so a large overdrive factor was originally included.

Figure 12 shows the modified voltage regulator / power supply stage of the single channel microstimulator, and Figure 13 shows the simulation results for these regulators along with the received voltage (16V peak, 1.5MHz) from a simulated telemetric link. It can be seen that the 4V supply is actually augmented to 4.45V by adding an additional diode drop in series with the Zener diode. The Zener diodes have a higher resistance because of their smaller area, and this would lead to increased ripple; however, this ripple is to a significant extent reduced by the use of Darlington pairs in both supplies. The Darlington pairs also help to reduce load dependence of the supply voltages by ensuring that sufficient current can be provided by the supplies with less base current drawn by the emitter follower current buffers. Thus the 4.4V supply has a ripple of about 5mV. The 9.5V supply has a ripple of about 0.2V, higher because of channel length modulation effects in the MOS current mirror that breaks down the 9.5V diode string. This effect has been reduced as much as possible through the use of very long channel devices, and additional diodes are included with the 9.5V Zener string to further boost this supply voltage. In total this stage uses about 350μA of current compared to the previous design's average of 1.6mA.

Table 7: Summary of current consumption in various generations of microstimulator (original single channel, redesigned single channel, and multichannel).

		CURRENT (μA)	
CIRCUIT BLOCK	NEW * 1 CHANNEL.	OLD * 1 CH.	MULTICHAN.
ENV. DET.	400	400	400
CLOCK	50	100	100
STIM. OUT	135	200	200
REGULATOR	350	1600	675
LOGIC / MISC.	750	750	1125
TOTAL	1685	3050	2500

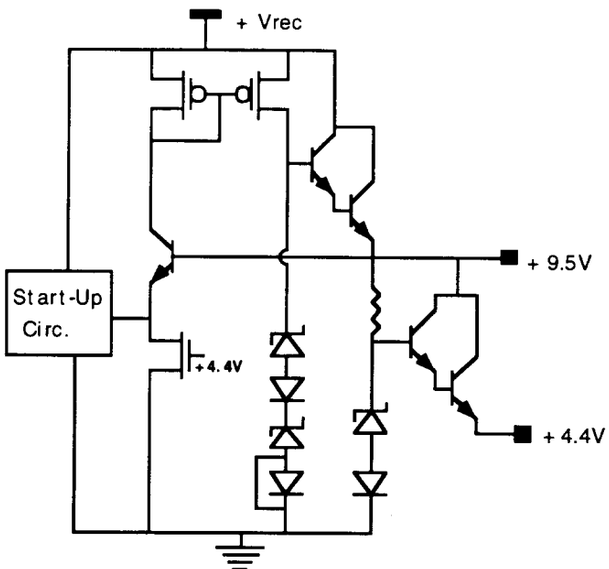

Figure 12: The modified voltage regulation / power supply stage for the single channel microstimulator is illustrated.

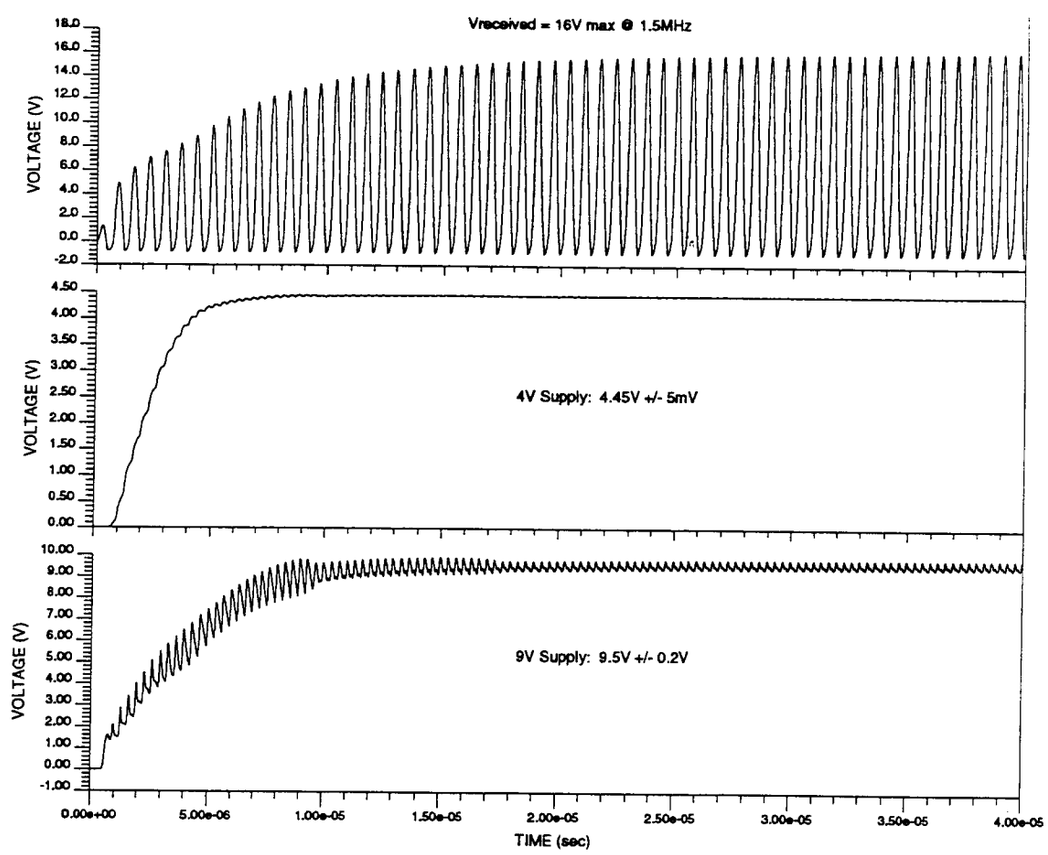

Figure 13: The simulated results of the redesigned voltage regulation circuitry, for a 16V peak, 1.5MHz carrier signal.

Stimulus Current Generation

The stimulus output stage is illustrated in Figure 14. Its primary features, as mentioned previously, are stable currents over a wide range of loads, higher compliance voltage than the previous single channel device's design, and programmability of the stimulus current amplitude. In the single channel device, software programmability (as in the multichannel device) would have been impossible without a considerable redesign of the logic control circuitry. Instead, it was chosen to allow hardwired programmability through laser-cut links (3 bits), to set the maximum current in seven steps of 1.43mA up to the 10mA in the base configuration. However, in this particular design it is also easy to make the maximum current deliverable greater than this base 10mA. This can be achieved by adding certain sized devices into the reference string used by the stage's operational amplifier to determine the current output. Thus this can also be achieved with simple laser cuts, tailored to a particular user's needs. The sizes of these devices and their effects on the maximum stimulus current for various configurations are shown in Table 8. It can be seen that the stage can deliver a maximum of 10.2mA to nearly 47mA in steps of roughly 5mA, and this can then be scaled down in seven hardwired steps. The stage can therefore deliver a total of 56 distinct current levels, theoretically. The true limitation will be how much current can actually be delivered by the driver device (not something that can be accurately modeled in SPICE, since the models will not account for breakdown effects adequately), and eventually such problems as electromigration, etc. The lines that will carry this current on the redesigned chip have been kept extra wide wherever possible to reduce such problems associated with limited current handling capability.

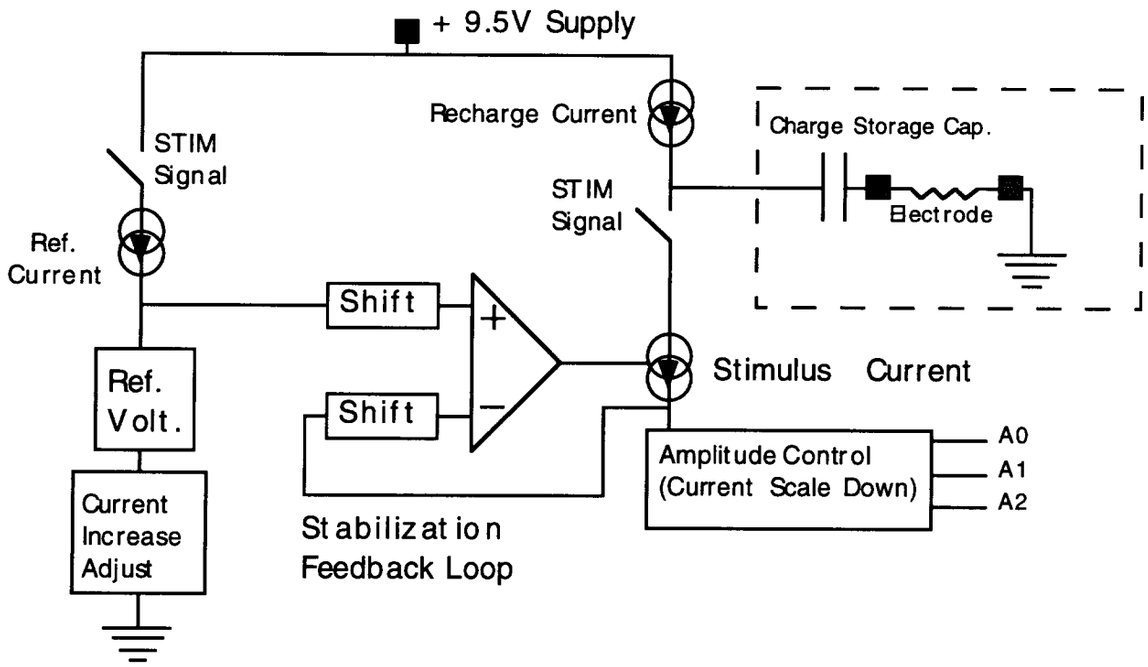

Figure 14: The modified stimulus current generation stage, with some detail omitted for clarity.

Table 8: Shows various laser trimmed configurations in the output stimulus stage and their effects on the maximum stimulus current (across 100Ω purely resistive load).

Devices Added in Reference String through Laser Cuts (μm /μm)	Output Stimulus Current (mA)
None	10.2 ± 0.6
14 /4	14.8 ± 0.6
14/8	19.85 ± 0.6
14/4, 14/8	24.5 ± 0.7
6/8	32.6 ± 0.9
6/8, 14/4	37.2 ± 1.1
6/8, 14/8	42.3 ± 1.2
All	46.9 ± 1.1

The ripple on these currents may appear significant initially, but it should be considered that these are results across a 100Ω purely resistive load. A more exact model of an electrode in tissue would include capacitive effects a well, which would smooth this ripple. Furthermore, as can be observed in Table 9 and Figures 15 and 16, the relative ripple for a given current level tends to decrease as the effective load is increased. The ripple also tends to decrease as the stimulus current is increased. Also observable in these figures is a slight lag (2μs) in the rise time of the stimulus current, due to the slew-rate limited charging of the large driver MOS' gate capacitance. Every effort was made to make the gain of the op amp in the stabilization loop high enough to get very predictable currents, but in so doing the power supply rejection ratio of the block as a whole may have suffered slightly and may have lead to this ripple as well as to the slightly lower slew rate. Nonetheless, with clever modifications, it was possible to reduce the stimulus turn on time from 15μs to the stated 2μs while keeping ripple fairly low and overall current consumption to about 135μA, (1/3) lower than the previous output current generator stages. Additionally, the stimulus current is much more broadly adjustable than in the previous single channel design and much more stable and predictable as well.

Table 9: The modified stimulus current generator has been shown in simulations to produce stable currents of variable amplitude through a wide range of loads.

LOAD (Ω)	**Current Expected (mA)**	**Current Observed (mA)**
100	1.43	1.48 ± 0.36
800	1.43	1.43 ± 0.3
100	5.7	5.84 ± 0.55
800	5.7	5.83 ± 0.2
100	10	10.2 ± 0.65
500	10	10.2 ± 0.225
800	10	10.12 ± 0.016
100	42	42.25 ± 1.18

Modified Envelope Detector

As mentioned previously, a redesigned envelope detector has been included on some single channel microstimulators and on the multichannel microstimulator. Since the design is a modification of the envelope detector used in the previous multichannel device, which has been discussed in previous reports, the envelope detector will not be discussed in depth here. It will only be said that the design is based upon differential inputs to a comparator when the incoming signal experiences transitions. The differential inputs are obtained by charging and discharging capacitors at different rates which are determined by the capacitor sizes at each input and their respective charge and discharge current sources. The discharge sources are always on, while the charging sources are on for a fraction of the rectified input voltage cycle. The resulting differential signal causes the envelope detector to transition and then settle as the capacitor voltages eventually become equal.

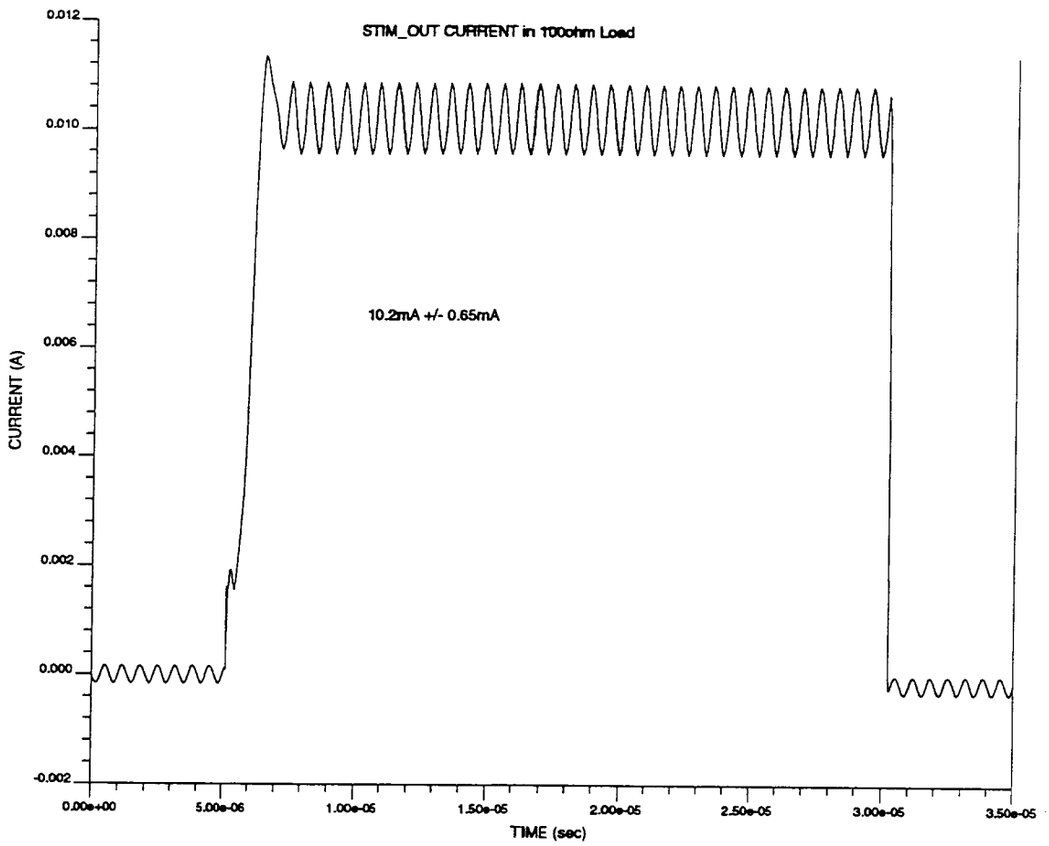

Figure 15: Stimulus current (10mA) across 100Ω load, showing ripple at carrier frequency.

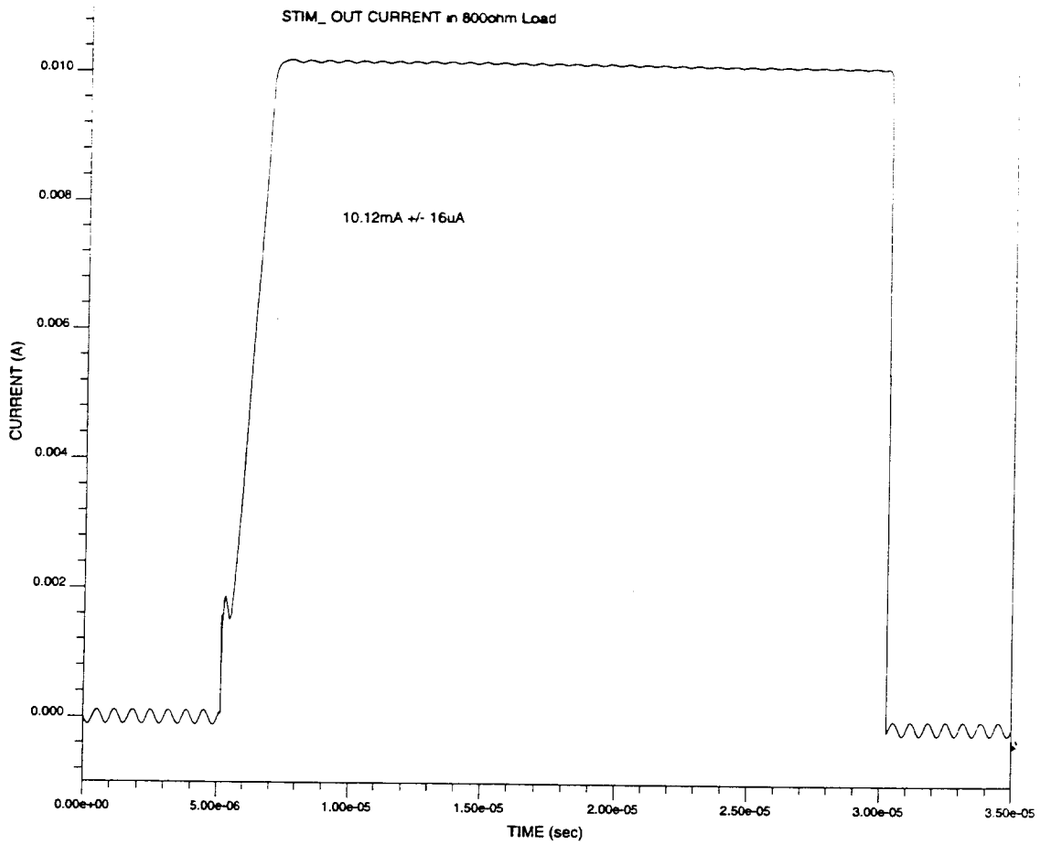

Figure 16: Stimulus current (10mA) showing outstandingly reduced ripple at higher loads (800Ω).

The main advantage of the new design stems from a reduction in capacitor sizes (leading to savings in both charge / discharge currents and die area) and from the great symmetry of behavior of the comparator structure used. This makes the envelope detector have very fast and equal response times to both high / low transitions and vice versa. Furthermore, this comparator has laser trimmable links to control its hysteresis (as did the previous multichannel stage), and the formula for this hysteresis is easy to understand. Thus, the comparator has very predictable behavior when adjusted by cutting these links, and the simulations on the envelope detector have corresponded extremely well to theoretical calculations. Thus the sensitivity of the envelope detector can be very controllably set to provide adequate noise immunity. The envelope detector has been found to work well up to at least 100KHz bit rates (with a 2V square wave modulation on a 15V maximum received signal).

Process Variation Simulations

In order to have confidence in the robustness of the overall system in the event of process variations during fabrication, simulations were conducted to examine the behavior of the principal blocks: supplies, envelope detector, clock, and stimulus current generator. The digital logic is in general quite robust and should not be greatly affected by process variations. Process changes were assumed to affect principally the KP (mobility x gate oxide capacitance/unit area) and (threshold voltage) of the MOS devices.

In the case of the voltage regulators, clock, and envelope detector, V_{To} changes of ± 25% were modeled. The clock was found to transition as expected normally, showing only slight

changes in the high and low fractions of each cycle. This robustness is most likely because the devices in the clock have been intentionally kept strong and with significant overdrive. The voltage regulators demonstrated slight but not significant changes in their levels. The 4.4V supply, for instance, whose stability is so critical to many portions of the chip, remained within ±0.1V or so of its normal operating point. The 9.5V supply showed a larger ripple and shifted downward in one case (when V_{To} of the PMOS devices was made more negative) to about 8.5V. This is understandable since a PMOS current mirror breaks down the diodes that create the 9.5V reference. Part of this shift, as well as some of the increased ripple, is due to the received voltage having been fairly low in this simulation, only about 13V maximum. Better results would be anticipated if the received voltage were closer to 15-18V. The envelope detector continued to work fine but required in one case a larger modulation depth (2.6V instead of 2V). This can easily be accommodated if the received voltage is kept at adequate levels.

The stimulus current generator was tested more extensively, modeling both KP and VTo changes, since fairly significant changes have been made to this stage and not fabricated yet. Two "worst cases" were envisioned, in which currents would generally be significantly higher or significantly lower than expected. For the sake of clarity, the results are summarized in Table 10. There the CURRENT HIGH STATE represents the case in which currents are generally higher, when KP is increased by 25% and V_{To} is made 25% more negative. This is in effect an "NMOS-strong" state. The other case is designated CURRENT LOW STATE and models a KP decrease of 25% and a shift in V_{To} by 25% in the more positive direction. This is in effect a "PMOS-strong" state, but generally in the circuit NMOS devices are used in current sources and PMOS devices are used to mirror these currents. Thus the currents in general can be expected to decrease. Also included for reference is the NOMINAL state without process variations. All results are across a 500Ω load, chosen because it is midrange among the load levels that can be driven by the microstimulator.

Table 10: Summary of results of process variations on stimulus current. Also listed are specific observations and their corrections.

	STIM. CURRENT (mA)	OBSERVATIONS / CORRECTIONS PRESCRIBED
CURRENT HIGH	14.2 ± 0.2	Initial, brief, high current surge (limited by compliance voltage). Can be kept < 5μs by trimming capacitor in STIM_OUT stage's op amp. Current can be scaled down if necessary.
NOMINAL	10.2 ± 0.2	No corrections needed; slew-rate limited for first 2μs.
CURRENT LOW	6.8 ± 0.054	May ring slightly for about 5μs before settling; ringing can be reduced by keeping cap in STIM_OUT stage high. Ringing will be attenuated by RC behavior of real electrodes / tissue. Can increase current if needed through laser-trimmed links.

Thus it can be seen that the stimulus current does vary as expected with large process variations, but the changes are neither catastrophic nor impossible to correct. Generally the same seems true for every analog and mixed mode block of the microstimulator.

Improved Operability Of Redesigned Microstimulator

As summarized in Table 7, the changes in various blocks of the microstimulator will lead to a 45% lower current in the single channel microstimulator (nearly 1.4mA lower than before) and up to nearly 400μA lower current in the multichannel device. These changes are expected to make it possible to operate microstimulators within a wide range of transmitter coil sizes, including coil sizes that were previously not usable though definitely desirable with our microstimulators. We have modeled the received voltage that we expect to obtain as a function of current demand in the receiver circuitry, for various transmitter coil diameters. Figure 17 illustrates these results. It can be seen that the single channel redesigned microstimulator should be able to operate even with 9cm diameter transmitter coils, receiving 16-17V peak. The multichannel device consumes a higher current and thus loads the link more but should still operate fine since the coupling should actually be better in the multichannel system which has a larger receiver coil. All of these cases were calculated for a 20 turn transmitter coil with length of 5cm, and a receiver coil with 100 turns on a ferrite core of 3mm length and 1.4mm total diameter. This receiver coil would fit inside the current glass package of the single channel microstimulator. In these results the transmitter supply voltage was also 12V, whereas if necessary this can be increased. For a 16V supply, for instance, a 38% increase in received voltage can be expected. On the other hand, as can be seen, with the smaller diameter transmitter coils, the transmitter supply voltage will actually have to be scaled down.

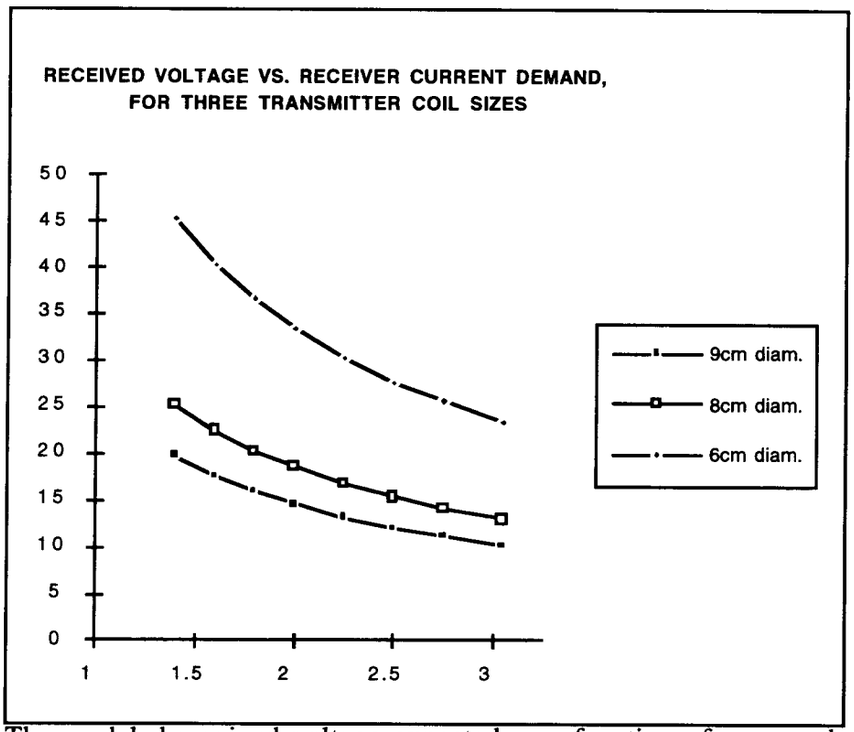

Figure 17: The modeled received voltage expected as a function of current demand in the receiver circuitry, for various transmitter coil diameters. The microstimulators fall in the 1.7-2.5mA range for single channel and multichannel devices, respectively.

Fabrication And Delivery Plans

These changes have thus been fully simulated and incorporated into the microstimulator layout. Masks are now being made to begin a new fabrication run by late July / early August, so that by October we should have new devices available for assembly and delivery. These devices should be much more reliable and should allow us to begin delivering working microstimulators as soon as we are able to assemble them after fabrication. Thus by the end of this year we should have results of several concurrent *in vivo* tests with collaborating groups.

3. ACTIVITIES PLANNED FOR THE COMING QUARTER

During the past quarter we made significant progress in two key areas. First, we continued to soak test packages and identified the major failure mode. In the coming quarter these tests will continue with the new silicon substrates. Although the results obtained so far may not be conclusive, they clearly indicate that these packages can survive in saline solutions for many decades. We will also continue to pursue to verify the validity of our accelerated models. Our future plans will concentrate on establishing a larger sample size for these accelerated soak tests.

Second, we will start the fabrication of the new microstimulators. Our main objective in this area is the delivery of fully functional, packaged devices to potential users of these devices. We believe that we are in a great position to accomplish this, now that all of the different components of the system has been tested.

Finally, we have also been working on the development of a miniature microstimulators for peripheral nerve stimulation by eliminating the hybrid coil and capacitor and using all on-chip components. This will provide a significant advance in the field of implantable microstimulators, and all of our preliminary designs and simulations show that this is possible. we have not yet reported on our activities in this area, and will do so as soon as more complete designs and preliminary experimental results are obtained. we expect to report on this area in our next progress report.